

Super-Eddington Accretion and Feedback from the First Massive Seed Black Holes

John A. Regan^{1*}, Turlough P. Downes¹, Marta Volonteri², Ricarda Beckmann²,
Alessandro Lupi², Maxime Trebitsch² & Yohan Dubois²

¹*Centre for Astrophysics & Relativity, School of Mathematical Sciences, Dublin City University, Glasnevin, D09 W6Y4, Ireland*

²*Sorbonne Universites, UPMC Univ Paris 6 et CNRS, UMR 7095, Institut d'Astrophysique de Paris, 98 bis bd Arago, 75014 Paris, France*

22 June 2022

ABSTRACT

Super-Eddington accretion onto massive black hole seeds may be commonplace in the early Universe, where the conditions exist for rapid accretion. Direct collapse black holes are often invoked as a possible solution to the observation of super massive black holes (SMBHs) in the pre-reionisation Universe. We investigate here how feedback, mainly in the form of bipolar jets, from super-Eddington accreting seed black holes will affect their subsequent growth. We find that, nearly independent of the mass loading of the bipolar jets, the violent outflows generated by the jets evacuate a region of approximately 0.1 pc surrounding the black hole seed. However, the jet outflows are unable to break free of the halo and their impact is limited to the immediate vicinity of the black hole. The outflows suppress any accretion for a free-fall time, thereby creating a feedback loop where high accretion rates generate strong outflows which temporarily suppress further accretion. The gas then cools, recombines and falls back to the centre where high accretion rates are again observed. The overall effect is to create an effective accretion rate with values of between 0.1 and 0.5 times the Eddington rate. If this episodic accretion rate is maintained for order 500 million years then the black hole will increase in mass by a factor of between 3 and 300 but far short of the factor of 10^4 required for the seeds to become the SMBHs observed at $z > 6$.

Key words: Cosmology: theory – large-scale structure – first stars, methods: numerical

1 INTRODUCTION

The discovery of super-massive black holes (SMBHs) with masses in excess of $10^9 M_\odot$ at redshifts greater than $z = 6$ (Fan et al. 2006; Mortlock et al. 2011) presents a significant difficulty for theories of black hole formation and growth. Black holes are expected to form as the end point of massive stars. Black holes forming from the first generation of massive Population III (PopIII) stars have initial seed masses close to their final stellar mass (Woosley et al. 2002, e.g.). However, these PopIII remnant black holes are expected to be born “starving” (Whalen et al. 2004; O’Shea et al. 2005; Johnson & Bromm 2007; Milosavljević et al. 2009; Alvarez et al. 2009). A more recent study by Smith et al. (2018) using a sample of approximately 15,000 PopIII remnant black holes from the Renaissance simulation suite (Xu et al. 2013; Chen et al. 2014; O’Shea et al. 2015) saw no evidence for significant accretion onto the remnant black holes with PopIII remnants increasing their mass by at most 10% over several hundred million years. The black holes are typically born into low density environments due to an initial supernova explosion which results in severely stunted growth. For PopIII stars within the direct collapse window (Heger et al. 2003)

the black hole initially experiences rapid accretion, however, the phase is short lived, with high density gas quickly consumed by further star formation. Even if PopIII remnant stars can remain in a region of high density, where local star formation is suppressed, a PopIII remnant would need to accrete at the Eddington limit for several hundred megayears in order to reach a mass of close to a billion solar masses by a redshift of 6. Such a scenario is very unlikely based on current research.

In light of this, several other pathways have been explored to attempt to understand the appearance of SMBHs in the first billion years of the Universe. The scenarios have broadly been divided into light seed scenarios and heavy seed scenarios. Light seed scenarios encompass mechanisms where the initial black hole mass is “light” ($M_{\text{init}} \sim 100 M_\odot$) but grows rapidly. The PopIII remnant case falls under the light seed scenarios, as do cases where initially light seeds rapidly merge together to form a more massive object. Several authors have considered a scenario where stellar collisions in high-redshift, dense star clusters lead to the runaway growth of a single star (Portegies Zwart et al. 2004; Gürkan et al. 2004, 2006; Freitag et al. 2006; Devecchi & Volonteri 2009; Katz et al. 2015; Habouzit et al. 2017). In this scenario, a dense stellar cluster becomes unstable to gravitational collapse leading to the merger of a significant number of the stars in the cluster and the formation

* E-mail: john.regan@dcu.ie, Marie Skłodowska-Curie Fellow

of a single massive star through mass segregation. The most massive stars which emerge from the cluster are expected to have initial masses of the order of $1000 M_{\odot}$.

Alternatively, there are a number of scenarios where a heavy seed ($M_{\text{init}} \gtrsim 10^4 M_{\odot}$) may emerge. In the centre of rapidly accreting atomic cooling haloes, which are metal-free, a supermassive star (SMS) is expected to form (Eisenstein & Loeb 1995; Bromm & Loeb 2003; Regan & Haehnelt 2009a,b). SMS formation requires very high accretion rates in excess of $0.01 M_{\odot}/\text{yr}$ (Begelman et al. 2006, 2008; Schleicher et al. 2013; Sakurai et al. 2016b) to inflate the envelope around the protostar and sustain a super-massive (or possibly a quasi) star (Hosokawa et al. 2013a,b; Woods et al. 2017; Haemmerlé et al. 2018, 2017). If accretion rates in excess of $0.01 M_{\odot}/\text{yr}$ can be sustained for the lifetime of the star then the star is expected to collapse into a massive black hole seed at the end of its lifetime, either through the General Relativistic instability (Chandrasekhar 1964) or after the star runs out of nuclear fuel. The final mass of the SMS is expected to be well in excess of $10^4 M_{\odot}$. The collapse into a direct collapse black hole then leaves a black hole seed with a large initial mass. If no supernova explosion occurs then the black hole can be born into a region with a plentiful supply of gas from which it can accrete.

Typically, the environmental conditions required for the heavy seed model require strong sources of nearby Lyman-Werner radiation, which can efficiently dissociate H_2 (Dijkstra et al. 2008, 2014; Visbal et al. 2014; Regan et al. 2017). However, dynamical processes which collisionally dissociate H_2 may also induce the correct environmental conditions for direct collapse black holes (Mayer et al. 2010; Inayoshi & Omukai 2012; Fernandez et al. 2014; Mayer et al. 2015; Inayoshi et al. 2015). Similarly, relative streaming velocities between baryons and dark matter following recombination (Tsaliakhovich & Hirata 2010) has been investigated by several authors in the context of the first massive black holes (Tanaka & Li 2014; Schauer et al. 2017; Hirano et al. 2017), with promising results. In summary, several pathways remain open to generating environmental conditions for the formation of massive black hole seeds.

Accretion onto the black hole in either scenario will determine the future growth of the black hole. The Eddington accretion rate can be derived by equating the gravitational force of a black hole to the radiative force experienced by the in-falling matter. The resulting force balance applies in the case of a spherically symmetric collapse, with the Eddington accretion rate given by

$$\dot{M}_{\text{Edd}} = \frac{4\pi G M_{\text{BH}} m_p}{\eta \sigma_T c} \quad (1)$$

where M_{BH} is the black hole mass, m_p is the proton mass, η is the radiative efficiency, σ_T is the Thomson scattering cross section and c is the speed of light. However, it is known that in non-spherically symmetric circumstances, the Eddington rate can be breached and super-Eddington accretion may persist. In this case, accretion can then proceed extremely rapidly. Numerous models of super-Eddington accretion exist. For example, the slim disk model of super-Eddington accretion was originally developed by Abramowicz et al. (1988) to investigate scenarios where the Eddington limitation could be broken. Super-Eddington accretion models of accretion onto stellar mass black holes have recently been investigated by a number of authors (Sądowski 2009; Sądowski et al. 2014; Sądowski & Narayan 2016; Sądowski et al. 2016; Jiang et al. 2017) with results consistently showing that super-Eddington accretion can be achieved.

Super-Eddington accretion has been shown, through numeri-

cal models, to generate powerful bipolar jets, which become active as the accretion rate exceeds the Eddington rate. These jets, though highly collimated, have the potential to shut off the very accretion flow that is driving the jets, and regulate the accretion flow to values sub-Eddington. Previous investigations have included only radiative feedback from BH seeds accreting at super-Eddington rates (Pacucci et al. 2015; Inayoshi et al. 2016; Lupi et al. 2016; Sakurai et al. 2016a; Toyouchi et al. 2018). In this work we investigate a scenario, where initial seed mass black holes accrete at or above the Eddington rate and generate bipolar jets.

2 NUMERICAL FRAMEWORK

In this study we have used the publicly available adaptive mesh refinement code *Enzo*¹ to study the birth of a massive black hole seed from a SMS. We have utilised the *SmartStar* particles introduced in Regan & Downes (2018a) and augmented them with subgrid prescriptions specific to a black hole seed as we now discuss.

2.1 Enzo

*Enzo*² (Bryan et al. 2014) is an adaptive mesh refinement code ideally suited to simulations of the high redshift universe. Gravity in *Enzo* is solved using a fast Fourier technique (Hockney & Eastwood 1988), which solves the Poisson equation on the root grid at each timestep. On subgrids, the boundary conditions are interpolated to the subgrids and the Poisson equation is then solved at each timestep. Dark matter is represented using particles, with each particle stored on the highest refinement grid available to it and thus the particle has the same timestep as the gas on that grid. The particle densities are interpolated using the cloud-in-cell technique onto the grid and solved at the same time as the gas potential. *Enzo* contains several hydrodynamics schemes to solve the Euler equation. To model the physics of jet launching, we use the Zeus hydrodynamic solver (Stone & Norman 1992a,b). A known limitation of the Zeus solver is the inclusion of artificial viscosity that can cause spurious heating of gas upstream from a shock front (Anninos & Norman 1994). However, the correct Rankine-Hugoniot jump conditions are nonetheless achieved. The very high resolution of our simulations and in particular the small number of cells over which jets are launched, goes some way towards mitigating these effects. Furthermore, the Zeus solver is very robust and able to follow the sharp discontinuities that arise as the jets are launched. Zeus is second order accurate in space and first order accurate in time. The Harten-Lax-van Leer with contact (HLLC) (Miyoshi & Kusano 2005) non-linear Riemann solver is used in conjunction with the Zeus solver.

Chemistry is an important component in following the collapse of (ideal) gas. We use the *Grackle*^{3,4} (Smith et al. 2017) library to follow the evolution of ten individual species: H , H^+ , He , He^+ , He^{++} , e^- , H_2 , H_2^+ , H^- and HeH^+ . We adopt here the 26 reaction network determined by Glover (2015a) as the most appropriate network for solving the chemical equations required by gas of primordial composition with no metal pollution and exposed to an external radiation source. The network includes

¹ <http://enzo-project.org/>

² Changeset:48882af312bc

³ <https://grackle.readthedocs.org/>

⁴ Changeset:482876c71f73

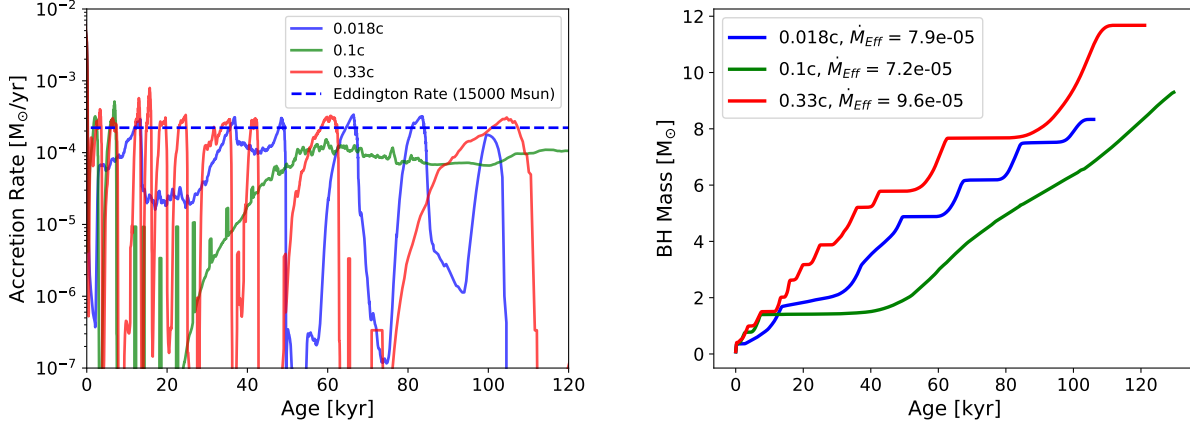


Figure 1. *Left Panel:* Mass accretion rates onto the black hole for different mass loading prescriptions. All simulations show that the jets effectively limit accretion to below the Eddington rate. Once accretion exceeds the Eddington limit the jets turn on disrupting the accretion flow. Differences between the impact of different prescriptions are clearly visible but similarities exist. The dynamical time for the highest density gas in the centre of the halo is a few thousand years and so gas falls back to the centre on this timescale. This is evident from the spikes for each prescription. *Right Panel:* The mass growth of each seed black hole. The initial mass of each seed is identical, $M_{seed} = 15904 M_{\odot}$. The effective accretion rate onto each seed is calculated over 100,000 years and found to be almost $\dot{M} \sim 10^{-4} M_{\odot}/\text{yr}$ in each case. This results in a mass increase of roughly $10 M_{\odot}$ in each case over the first 100,000 of the seed black holes existence.

the most up-to-date rates as described in Glover & Jappsen (2007), Glover & Abel (2008), Glover & Savin (2009), Coppola et al. (2011), Coppola et al. (2012), Glover (2015a), Glover (2015b), Latif et al. (2015). The cooling mechanisms included in the model are collisional excitation cooling, collisional ionisation cooling, recombination cooling, bremsstrahlung and Compton cooling off the cosmic microwave background.

2.2 Simulation Setup

The simulation explored here is the “Ref20.100J21_OT” simulation from Regan & Downes (2018b), hereafter R18b. This simulation used a Lyman-Werner background of $100 J_{21}$ to dissociate H_2 and allowed for the formation of an atomic cooling halo in which a SMS can form. The SMS formed at a redshift of $z = 24.7$. The maximum resolution of the simulation was set to 0.00025 pc ($\sim 50 \text{ au}$). At this resolution, resolving the outer envelope of the SMS becomes possible. In R18b the simulation was run for 250 kyrs at which point a single SMS was accreting at approximately $10^{-2} M_{\odot}/\text{yr}$ (see Figure 2 from R18b) and had achieved a mass of approximately $15,000 M_{\odot}$. We begin the simulation for this study from this point. We briefly review the original simulation for completeness.

The original simulation was run within a cosmological box of $2 h^{-1} \text{ Mpc}$ (comoving), on a root grid of 256^3 and with three levels of nested grids. The grid nesting and initial conditions were created using MUSIC (Hahn & Abel 2011). Within the most refined region (i.e. level 3) the dark matter particle mass is $\sim 103 M_{\odot}$. In order to further increase the dark matter resolution of our simulations, we split the dark matter particles according to the prescription of Kitsionas & Whitworth (2002), as described in Regan et al. (2015). We split particles centered on the position of the final collapse as found from lower resolution simulations within a region with a comoving side length of $43.75 h^{-1} \text{ kpc}$. Each particle is split into 13 daughter particles resulting in a final high resolution region with a

dark matter particle mass of $\sim 8 M_{\odot}$. The particle splitting is done at a redshift of 40, well before the collapse of the target halo. Convergence testing to study the impact of lower dark matter particle masses was discussed in Regan et al. (2015).

The baryon resolution is set by the size of the grid cells. In the highest resolution region this corresponds to approximately $0.48 h^{-1} \text{ kpc}$ comoving (before adaptive refinement). Setting the maximum refinement level for this simulation to 20 results in a maximum resolution of 0.00025 pc . As is standard in simulations of this type, refinement is triggered in Enzo when certain user defined thresholds are exceeded. The refinement criteria used in this work were based on three physical measurements: (1) The dark matter particle over-density, (2) the baryon over-density and (3) the Jeans length. The first two criteria introduce additional meshes when the over-density of a grid cell with respect to the mean gas or dark matter density exceeds 8.0. Furthermore, we set the *Minimum-MassForRefinementExponent* parameter to -0.1 making the refinement more aggressive for the baryon and dark matter over-density and hence making the behaviour of the adaptive mesh “super-Lagrangian” in nature (see Bryan et al. (2014) for further details). This technique also reduces the threshold for refinement as higher densities are reached. For the final criteria we set the number of cells per Jeans length to be 32 in these runs.

In order to suppress PopIII star formation and allow the simulation to form pristine atomic cooling haloes, we imposed an artificial Lyman-Werner background. We set the effective temperature of the background radiation field to $T_{\text{eff}} = 30000 \text{ K}$. This background temperature suitably models the spectrum of a population of young stars (Wolcott-Green & Haiman 2012; Sugimura et al. 2014; Latif et al. 2015). The effective temperature of the background is important as the radiation temperature determines the dominant photodissociation reaction set in the irradiated halo. This in turn leads to a value of J_{crit} - the flux above which complete isothermal collapse of the irradiated halo is observed due to the complete suppression of H_2 .

As the gas density increases in high density regions, hydro

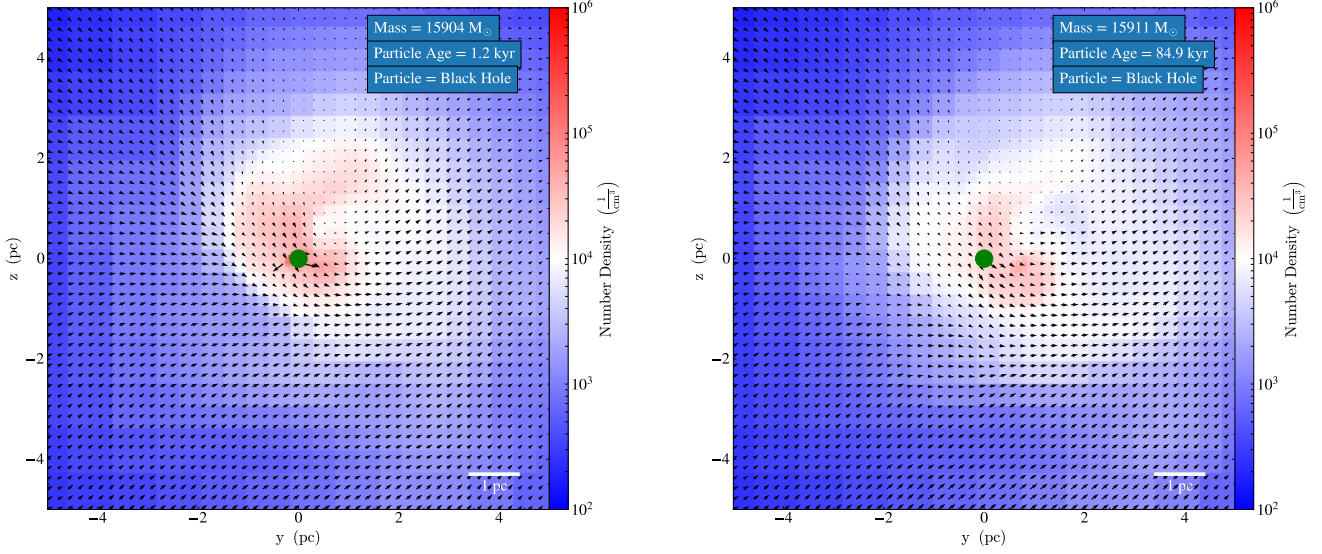


Figure 2. The number density of the gas in a 10 pc volume surrounding the black hole. The velocity of jets in this projection is 6000 km s^{-1} . The velocity of the jets is marked with arrows to give the direction. As the accretion rate exceeds the Eddington rate bipolar jets are launched from around the black hole (e.g. in the left hand panel). The gas density surrounding the black hole (and thus available) for accretion diminishes noticeably as time proceeds from left to right. Note that the radial extent of the black hole (shown in green) has been greatly exaggerated for this plot.

codes, including *Enzo*, require a method to convert the high density gas into stars in many cases. This is done to deal with gas which has reached the maximum allowed refinement level of the simulation and for which further collapse is being artificially suppressed through artificial pressure support. Within the “Ref20_100J21_OT”, simulation particles were introduced once the following criteria were met:

- (i) The cell is at the highest refinement level
- (ii) The cell exceeds the Jeans density
- (iii) The flow around the cell is converging along all axes
- (iv) The cooling time of the cell is less than the freefall time
- (v) The cell is at a local minimum of the gravitational potential

As described in R18, all “stars” which form are initially assumed to be stars with low surface temperatures that are appropriate for main sequence SMSs and less massive proto-stars on the Hayashi track. As long as the accretion rate remains above a critical value of $\dot{M}_* \gtrsim 0.04 \text{ M}_\odot/\text{yr}$ (Sakurai et al. 2016b), the star remains a SMS. If the accretion rate drops below this critical value, the star contracts and becomes a PopIII star. In “Ref20_100J21_OT”, the accretion rate dropped below the critical value shortly after formation, after approximately 25 kyrs. Nonetheless, the accretion rate remained high even though the ionising radiation from the PopIII was able to ionise and heat some of the gas immediately surrounding the proto-star. Similar results were observed in the simulations of Chon et al. (2017). The accretion rate remained relatively constant at around $\dot{M}_* \sim 0.01 \text{ M}_\odot/\text{yr}$ for the duration of the simulation (~ 250 kyrs). At this point we now allow the massive PopIII star to transition to a massive black hole seed. Ideally, we would have allowed the PopIII to continue to accrete until it either ran out of nuclear fuel (after $\sim 10^6$ years) or reached the GR instability (after reaching a mass of $M_{SMS} \sim 5 \times 10^5 \text{ M}_\odot$). However, the computational expense in running the simulation at this refinement level is extreme and the physics of massive PopIII star evolution is insufficiently understood to pursue this course. Instead we, pre-

turely, convert the star particle into a black hole particle in order to study the impact that this change will have on the surrounding material and the accretion onto the black hole.

2.3 Accretion onto the black hole

The accretion onto the black hole particle is similar to the accretion mechanism used to accrete onto the star particle. The particle can accrete gas within its accretion radius (4 cells) and it can merge with other *SmartStar* particles. Accretion onto the *SmartStar* is determined by calculating the flux of gas across the accretion surface.

$$\dot{M} = 4\pi \int_S \rho v_r^- r^2 dr \quad (2)$$

where \dot{M} is the mass accretion rate, S is the surface over which we integrate, ρ is the density of the cells intersecting the surface, v_r^- is the velocity of cells intersecting the surface and which have negative radial velocities and r is our surface’s radius. The surface, S , is the surface of a sphere with radius the accretion radius. As noted above we set the accretion radius to be 4 cells, we choose to fix this radius independently of the resolution or the mass of the *SmartStar*. We do this so as to be as accurate as possible when calculating the accretion rate, any mass travelling radially inward at a distance of four cells from the *SmartStar* is taken to be accreted onto the *SmartStar* - we therefore strive for the maximum possible physical resolution.

As an alternative to directly measuring accretion using the mass flux method described above we can also calculate the accretion rate on the black hole using the Bondi-Hoyle prescription. As described in Krumholz et al. (2004) we use the following approximate formula

$$\dot{M} = 4\pi \rho_\infty r_{BH}^2 (\lambda^2 c_\infty^2 + v_\infty^2)^{1/2} \quad (3)$$

where ρ_∞ is the density of gas at the Bondi-Hoyle radius, r_{BH} is the Bondi-Hoyle radius, c_∞ is the sound speed at infinity (in the

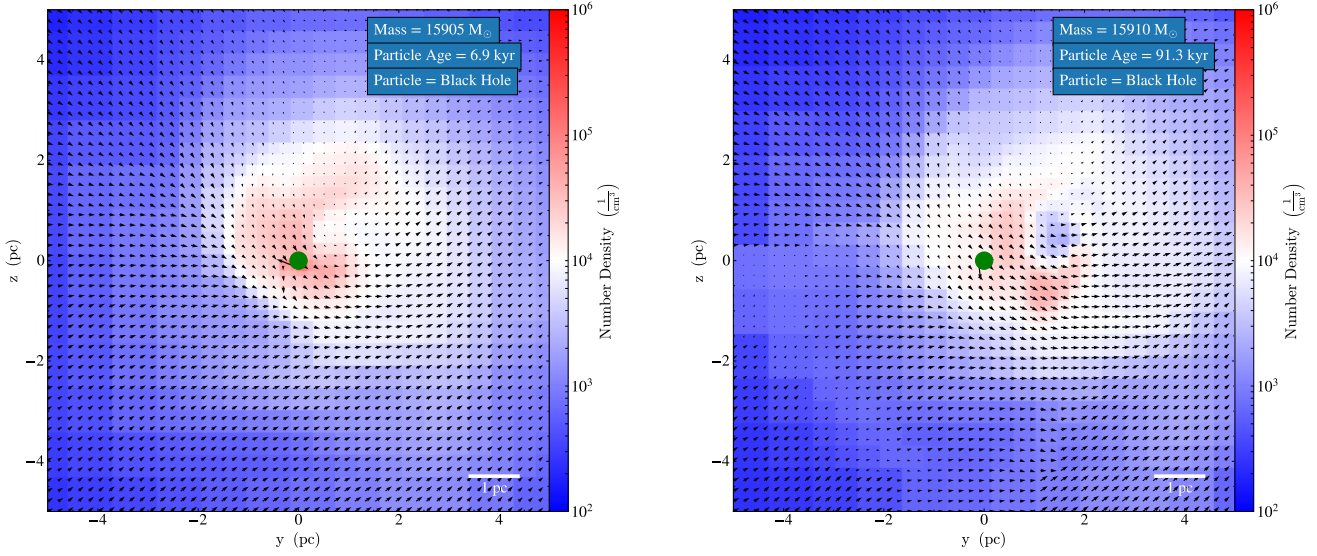


Figure 3. The same as Figure 2 except for the simulation with jet velocities of $30,000 \text{ km s}^{-1}$. Jets diminish the initial gas supply available for accretion.

host cell in this case) and v_∞ is also the relative velocity of the sink particle and the gas in the host cell of the black hole. λ is a constant of order unity. While, at the high resolution we are able to evolve our simulations at, the mass flux approach is more accurate we use the Bondi-Hoyle prescription immediately after jets are launched. We do this to prevent the procedure from calculating spurious accretion rates due to the large mechanical feedback from the jets. After 50 further timesteps the accretion procedure automatically reverts to the mass flux method.

The accretion onto the star is calculated at each timestep, however this is likely to be a very noisy metric. To alleviate this to some degree we average the accretion rate over hundreds of timesteps typically corresponding to between 10 and 100 years. The average accretion rate is then used as the actual accretion rate. The accretion rate is added as an attribute to each star and hence a full accretion history of every `SmartStar` is outputted as part of every snapshot.

In order to accrete gas onto the `SmartStar` gas must be removed from the grid. In order to do this we follow the prescription advocated by [Krumholz et al. \(2004\)](#) where a kernel weighting is applied to cells within the accretion radius of the particle. The equations used to assign this weighting can be found in [Krumholz et al. \(2004\)](#), equations 13 and 14.

Mergers with other `SmartStars` are also included in the accretion onto the `SmartStar`. In this case the more massive `SmartStar` retains its information (i.e. age, type etc) after the merger event - information on the less massive `SmartStar` is lost. The mass of the less massive `SmartStar` is added to the accretion rate of the more massive `SmartStar` for that timestep. `SmartStars` are merged when they come within an accretion radius of each other.

2.4 Feedback from the black hole

The feedback from an accreting black hole is primarily determined by the radiative efficiency of the disk, η_{disk} . η_{disk} is typically set to a value close to 0.1 for a non-rotating black hole. For these sim-

ulation we use a value very close to this, $\eta_{disk} = 0.103$, which we derive by explicitly accounting for the spin of the black hole (e.g. [Sądowski & Narayan 2016](#))

$$\eta_{disk} = 1 - \sqrt{1 - \frac{2.0}{3.0 R_{ISCO}(a)}} \quad (4)$$

where a is the spin parameter of the black hole which we set to $a = 0.7$ and R_{ISCO} is a parameterisation of the inner most stable orbit given by [Abramowicz & Fragile \(2013\)](#)

$$R_{ISCO} = R_G * \left(3 + Z_2 - [(3 - Z_1) * (3 + Z_1 + 2Z_2)]^{\frac{1}{2}} \right) \quad (5)$$

where $Z_1 = 1 + (1 - a^2)^{1/3} \left((1 + z)^{1/3} + (1 - a)^{1/3} \right)$,

$Z_2 = \left(3 * a^2 + Z_1^2 \right)^{1/2}$ and R_G is the gravitational radius, $R_G = GM/c^2$. The accretion rate onto the black hole must now be modified to account for the energy that is returned to the outer medium from the accretion

$$\dot{M}_{BH} = \dot{M} * (1 - \eta_{disk}) \quad (6)$$

where \dot{M}_{BH} is now the mass accretion rate onto the black hole while \dot{M} is the numerically determined accretion rate onto the black hole as described in §2.3. The feedback from the black hole can now be further decomposed into radiative feedback from the disk and mechanical feedback from a jet component.

2.4.1 Radiative Feedback

To model the radiative feedback from the black hole we assume a multi-colour disk for the accretion disk and then a fit a corona with a power law (e.g. [Done et al. 2012](#)). We divide the energy radiated equally between the multi-colour disk and the power law component. The radiative feedback within `Enzo` is modelled using the ray tracing module `MORAY` ([Wise & Abel 2011](#)), which discretises the radiation into a set of finite energy bins which are then transported outwards from the black hole particle. We split the radiation into five energy bins from infrared up to hard X-rays. The energy bins used are 2.0 eV, 12.8 eV, 19.1eV, 217.3 eV and 5190

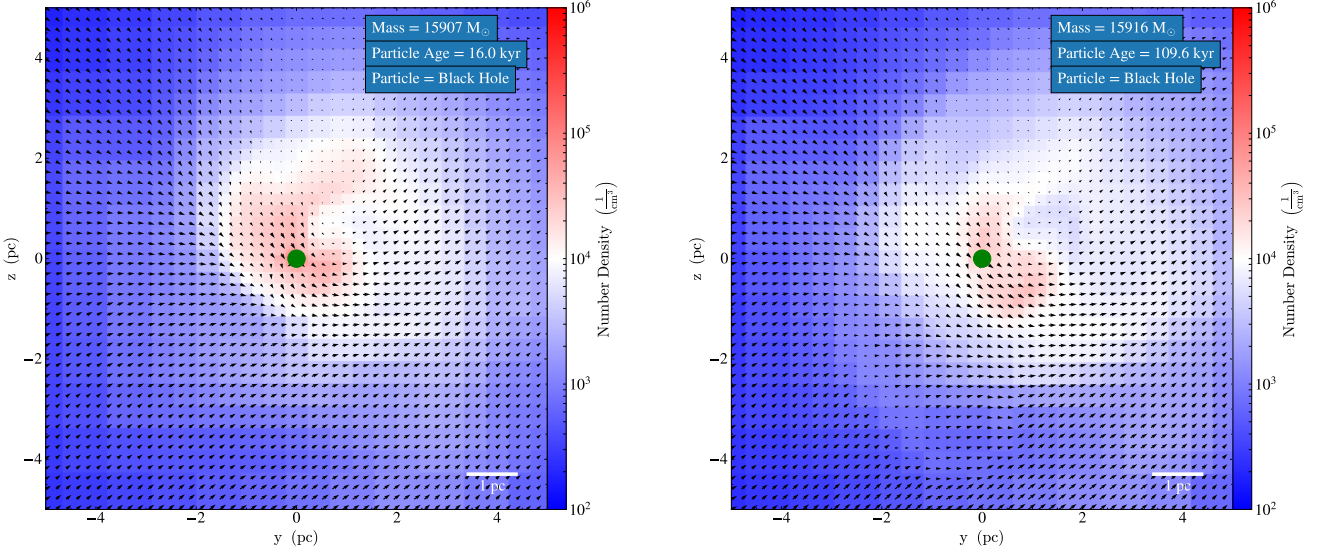


Figure 4. The same as Figures 2 and 3 except for the simulation with jet velocities of $100,000 \text{ km s}^{-1}$.

eV with the actual value of the luminosity at each timestep determined by the accretion rate at that timestep. The fractional energy in each energy bin is then determined by the accretion rate onto the black hole and the mass of the black hole. For super-Eddington adjustments to the radiative feedback we employ the fit from [Madau et al. \(2014\)](#) who themselves use [Sądowski \(2009\)](#) to derive the fit. In this case the luminosity is calculated as

$$\frac{L}{L_E} = A(a) \left(\frac{0.985}{\dot{M}_E/\dot{M}_{BH} + B(a)} + \frac{0.015}{\dot{M}_E/\dot{M}_{BH} + C(a)} \right) \quad (7)$$

where the functions A, B, C scale with the spin of the black hole, a , as

$$A(a) = (0.9663 - 0.9292a)^{-0.5639} \quad (8)$$

$$B(a) = (4.627 - 4.445a)^{-0.5524} \quad (9)$$

$$C(a) = (827.3 - 718.1a)^{-0.7060} \quad (10)$$

and \dot{M}_E is the Eddington mass accretion rate. The luminosity per solar mass is adjusted in this case compared to the thin disk model but the energy bins and energy fraction per bin remain unchanged. In essence the radiative efficiency is reduced, as expected.

For the cases considered here we limit the radiative feedback component to non-ionising radiation only - i.e. we use the first two energy bins of our model only. We do this for three reasons. Firstly, the simulations are computationally expensive and in order to reduce the computational expense we limit the radiative feedback to being optically thin and below the ionisation potential of hydrogen. Secondly, the fraction of energy emitted as ionising radiation falls off rapidly as the accretion rate decreases and by considering only the infrared and Lyman-Werner components we are nonetheless still capturing the bulk of the radiative processes. Finally, in this work we are primarily interested in investigating the impact of mechanical feedback (i.e. jets) on the ability of seed black holes to accrete effectively and hence neglecting the ionising radiation component allows us to do that. A full treatment of the radiative feedback will be considered in an upcoming study.

2.4.2 Mechanical Feedback

Microphysical models of the physics of accretion disks have shown that bipolar jets produced predominantly by the tangling of magnetic field lines are a robust feature of super-Eddington accretion. Jets appear to also be present at low accretion rates, most frequently when the accretion rates falls below $10^{-3} \dot{M}_{Edd}$ (e.g. [Merloni & Heinz 2008](#); [Sądowski & Narayan 2016](#), and references therein), but in this paper we want to focus on the effects of jets launched during super-Eddington phases, therefore we do not initiate jets for accretion rates below the Eddington rate and instead all of the feedback is radiative in that case (below the ionisation threshold of hydrogen as discussed above).

To calculate how much energy is mechanical output in the super-Eddington regime, we again follow the models of [Sądowski & Narayan \(2016\)](#). In this case the total jet luminosity is given by

$$L_{jet} = \eta_{jet} \dot{M}_{BH} c^2 \quad (11)$$

where η_{jet} is the jet efficiency factor given by ([Sądowski & Narayan 2016](#))

$$\eta_{jet} = 1.3a^2 \quad (12)$$

This efficiency assumes maximum efficiency of the jet, where we have assumed a “MAD” value of 1, making this an upper limit to the jet efficiency [Sądowski & Narayan \(2016\)](#). An additional complication in modelling jets is that jets are an inherently relativistic phenomenon and their launch speed is close to the speed of light. Furthermore, the jets are launched on scales close to R_G which is far below the resolution of our simulations. Therefore, modelling both the speed and the initial launch radius of the jet are beyond the capabilities of ENZO. Hence we “mass load” the jet (e.g. [Ciotti & Ostriker 2001](#); [Dubois et al. 2012](#)) by adding additional mass to the jet and by reducing the speed of the jet. This accounts for the assumption that the speed of the jet will diminish as the jet entrains mass on its way from the black hole. The mass loading factor, β_{jet} , is defined as

$$\beta_{jet} = \frac{\dot{M}_{jet}}{\dot{M}_{BH}} \quad (13)$$

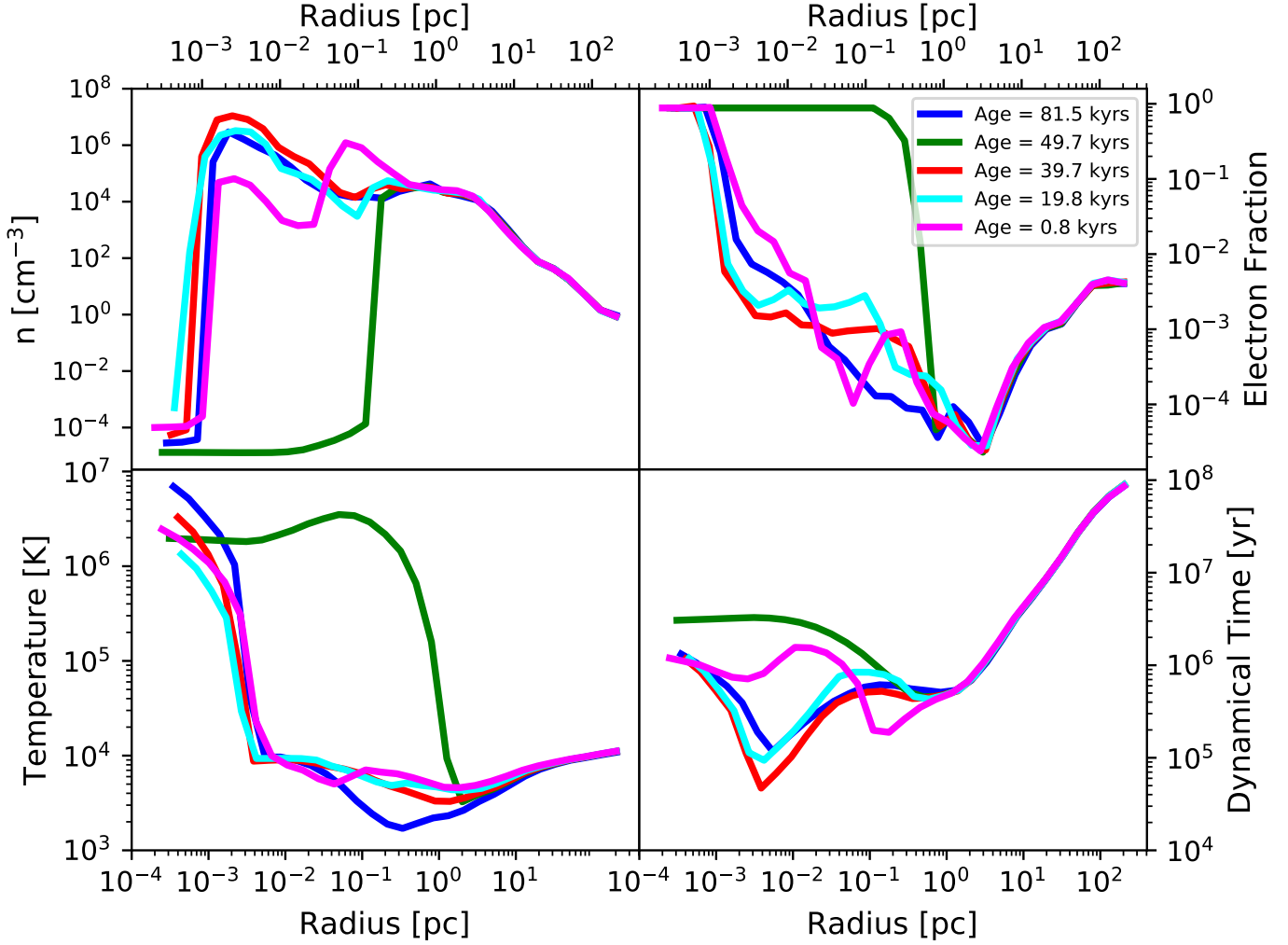


Figure 5. Radial profile plots of the number density, temperature, electron fraction and dynamical time of the gas at times between seed black hole formation and the end of the simulation after 100,000 years. The impact of the jets is clearly seen in the green line in this figure (compare the time to Figure 1). At age ~ 49.7 kyr the accretion rate exceeds the accretion rate driving a jet and mass outflow at $6,000 \text{ km s}^{-1}$. The temperature rapidly increases to over 10^6 K, the density of the gas drops rapidly as gas is driven out from the centre of the halo and the gas that remains is strongly ionised. The dynamical time of the gas left in the centre increases proportionately. Nonetheless, the gas is able to cool and fall back into the centre. This is shown by the blue line where the densities in the centre have recovered and the temperatures have returned to close to 10^4 K.

where \dot{M}_{jet} is the amount of material ejected by the jet per unit time and again \dot{M}_{BH} is the mass projected to accrete onto the black hole surface. We now define the jet 'kinetic' power, KE_{jet} , as in Kim et al. (2011) and equate it to the luminosity of the jet using conservation of energy to write

$$KE_{jet} = \frac{1}{2} \dot{M}_{jet} v_{jet}^2 \quad (14)$$

$$KE_{jet} = L_{jet} \quad (15)$$

we can then equate the mass loading factor, β_{jet} , with the velocity of the jet, v_{jet} , and write

$$\beta_{jet} = 2\eta_{jet} \frac{c^2}{v_{jet}^2} \quad (16)$$

and we see that the mass loading of the jet and the velocity of the jet are degenerate as expected. Typically, in numerical simulations v_{jet} is set to be much less than c . For example setting $v_{jet} = 0.1c$ gives $\beta_{jet} = 127.4$ while $v_{jet} = 0.01c$ gives $\beta_{jet} = 12740$. In both

cases $\beta_{jet} \gg 1$.

Attempting to mass-load the jet by factors of up to 10^5 can be problematic as there may not be enough mass in the surrounding cells to do so. In this, rather common, case we adjust the mass accretion rate onto the black hole so that the black hole can effectively only accrete for a fraction of the current timestep. The fraction is calculated so there is sufficient mass to load the jet. Ideally, we would like to decrease the timestep of the simulation such that the total mass required for a single accretion + feedback episode, i.e. $M_{tot} = \Delta M_{BH} + \Delta M_{jet} = (1 + \beta_{jet}) * M_{BH}$ is less than the total mass available in the accretion region i.e. $< M_{acc}$ where $\Delta M_{BH} = \dot{M}_{BH} \Delta t$. Practically, this will make the timestep unaffordably short, particularly in the super-Eddington accretion regime, where both the amount of mass removed from the grid, and the total energy to be returned to the grid, will be high. Instead we decrease the accretion time in this subgrid manner. We do this by introducing a factor, ϵ_t , which operates on the accretion rate modifying both the actual accretion rate found for the black hole and the

resulting jet ejection rate. ϵ_t is calculated as

$$\epsilon_t = \min(1.0, \frac{\dot{M}_{acc}}{\dot{M}} \frac{1.0}{1 - \eta_{disk}} \frac{1.0}{1 + \beta_{jet}}) \quad (17)$$

The above equation ensures mass conservation within the subgrid algorithm with ϵ_t fixed to be always less than one. A further consequence of this approach is that the ejected mass is very similar in all cases independent of the speed of the jet. Consider the following:

$$\dot{M}_{jet} = \beta_{jet}(1 - \eta_{disk})\dot{M} \frac{\dot{M}_{acc}}{\dot{M}} \frac{1.0}{1 - \eta_{disk}} \frac{1.0}{1 + \beta_{jet}} \quad (18)$$

$$\dot{M}_{jet} = \frac{\dot{M}_{acc}}{\frac{1}{\beta_{jet}} + 1} \quad (19)$$

$$\dot{M}_{jet} \sim \dot{M}_{acc} \quad \text{for } \beta_{jet} \gg 1 \quad (20)$$

hence we have found that the mass ejected by the jet will be close to, but always less than, the mass in the surrounding accretion sphere. This is expected since we need ϵ_t to be such that there is always sufficient mass available to mass load the jet.

Now that the algorithm for determining the mass of the jet and the speed of the jet has been determined, it remains to describe how the jets are launched within the simulation. In this regard we follow both Kim et al. (2011) and Dubois et al. (2012). Kim et al. (2011) use “supercells” within the Enzo grid hierarchy to launch the jets, effectively adding mass and velocity to cells on the outer edge of a cone to launch the jet. As recommended by Dubois et al. (2012) we insert the jet at the maximum resolution and over the minimum number of cells as possible so as to have the jet as collimated as possible. Typical jets are observed to be less than 1000 R_G (e.g. Doeleman et al. 2012) and so well below the resolution of our simulations - hence we insert the jet over a limited number of cells (27). The effect of this is to make the jet denser relative to spreading the jet over a larger number of cells - the typical density of the jets launched in our simulations is $\rho_{jet} \sim 10^{10} \text{ cm}^{-3}$.

2.5 Simulation Realisations

In order to test different mass loading values we select three different jet velocities. The speed of the jet impacts the mass loading value through equation 16. Jets due to super-Eddington accretion rates are launched at relativistic speeds, however, modelling relativistic jets is computationally challenging and so mass loading the jet is often preferred. In this study we examine three different jet launching speeds: (1) 6,000 km s^{-1} (2) 30,000 km s^{-1} and (3) 100,000 km s^{-1} . These speeds correspond to 0.018c, 0.1c and 0.33c. As outlined in equation 20, the mass ejected by the jet during each outburst is similar in all cases. Therefore, the difference between each realisation is effectively only in the speed of the jets and hence the momentum and energy of the jets in each realisation. As we will see, all three realisations result in similar effective accretion rates regardless of the jet speed chosen.

3 RESULTS

Our goal in this study is to examine the earliest stages of seed black hole growth immediately after the SMS or massive PopIII collapses into a black hole. As was found in the SMS simulations in R18 the accretion rate onto the massive PopIII star after 250 kyr is approximately 0.01 M_\odot/yr . However, feedback from an accreting black hole is much more powerful than that of a SMS or a massive PopIII star due to the significantly enhanced compactness of the black

hole. We here investigate primarily the impact of the mechanical feedback on future accretion.

In Figure 1 we plot the mass accretion rate and the total mass accreted by the black hole. In the left hand panel we plot the mass accretion rate over the first 100,000 years after the seed black hole forms for three different values of jet velocity. The impact of the jets is clearly visible. Jet events are immediately followed by periods of very low accretion before gas cools and falls back to the centre of the potential again. The periods of high accretion, which generate the jet events, are episodic with periods of between a few kiloyears and 20 kiloyears approximately. The dynamical time of high density gas in these simulations is a few tens of kiloyears consistent with the cycles of accretion found here.

The green line, jets with launch velocities of 0.1 c, shows a slightly different behaviour to the two other realisations. In the case of the jet with velocities of 0.1 c initial periods of super-Eddington accretion are followed by a very large drop in accretion before it gradually rebuilds again. After the first two periods of super-Eddington accretion the gas never again falls in at sufficient rates to generate jets and instead the accretion remains relatively steady at approximately $10^{-4} M_\odot/\text{yr}$. It is interesting that the jets with both higher and lower launch speeds show qualitatively different behaviour and it highlights the variability of such systems. After the gas is expelled from the central object it does fall back again, on approximately the dynamical time, but it need not necessarily, fall back at the same rates. Also this behaviour is shown to not be directly correlated with the launch speed.

In the right hand panel we plot the total mass accreted by the black hole against time. We calculate the effective accretion rate simply by taking the initial black hole mass from the final black hole mass divided by the time. The effective mass accretion rate is less than $10^{-4} M_\odot/\text{yr}$ in all cases. This is two orders of magnitude below the accretion rate onto the massive PopIII star immediately prior to collapse into the black hole. Over the course of 100,000 years the black holes grow by only approximately 10 M_\odot in each realisation. If accretion at this rate were to continue, the black holes would increase their mass by only one order of magnitude over one billion years. They would grow to become intermediate mass black holes with masses of $M_{BH} \sim 10^5 M_\odot$ in the early Universe.

In Figure 2, Figure 3 and Figure 4 we plot projections of the number density in a 10 pc cube surrounding the black hole. Overplotted on top of the density field is the velocity field with directional arrows. The length of the arrows is proportional to the value of the velocity at that point. The plots are made near the start and near the end of each simulation. Initially, in the left hand panels, we see the black hole (marked in green) surrounded by high density gas with strong outflows due to jet events. As the simulations proceed gas is driven out of the central regions and must fall back in order for accretion to pick up again. The free fall or dynamical time is given by

$$t_{ff} = \sqrt{\frac{3}{32G\rho}} \quad (21)$$

where ρ is the gas density. For our system this corresponds to 10 kyr at a radial distance of 0.01 pc from the centre of the halo down to less than 1 kyr for the highest density gas at the very centre of our halo. In each case what is immediately noticeable is that the outflows from the jets have little or no effect on gas outside of approximately 1 pc. In each realisation there is no fingerprint from the jet activity at scales larger than this even though the jets are launched with velocities of up to 100,000 km s^{-1} . The inflow from the gas is easily able to overwhelm the jet momentum, so that while

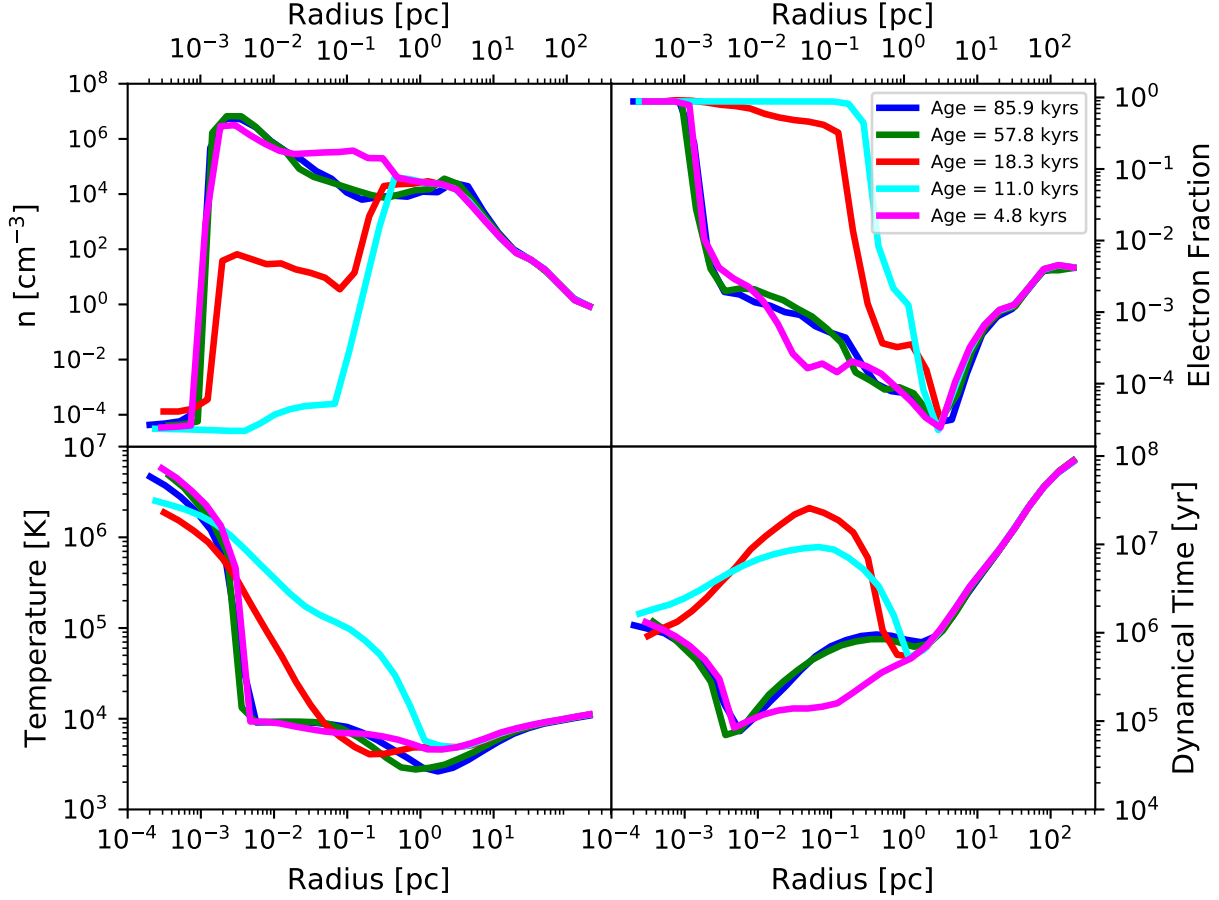


Figure 6. The same as Figure 5 for the $30,000 \text{ km s}^{-1}$ simulation. In this case we show the effect of a strong initial jet at age $\sim 11 \text{ kyr}$ which drives gas away from the centre of the halo. Nonetheless, the gas recovers and can fall back into the centre, again reactivating accretion, within a few kiloyears triggering further bursts of feedback.

the jets are able to effectively shut off accretion in the immediate radius of the black hole they have no effect on the gas at scales of a parsec or larger.

In Figures 5, 6 and 7 we quantify the projection plots by taking radial profiles for different times during the course of the simulation. Focusing first on the simulation with jet velocities of $6,000 \text{ km s}^{-1}$ (i.e. Figure 5) we see that jet events reduce the density of the gas by nearly ten orders of magnitude out to a distance of approximately 0.1 pc . The very low density gas that is left behind is superheated to a temperature of 10^6 K and the gas is also fully ionised. Nonetheless the gas is quickly able to recover and fall back into the centre of the potential and in a little over 10 kyr the gas has reached sufficient density that the black hole can accrete at very high rates and can indeed again exceed the Eddington rate (see Figure 1).

Figures 6 and 7 show both qualitatively and quantitatively similar results. Periods of super-Eddington accretion launch jets, which drive high density gas out from the centre of the halo. The density of the gas surrounding the black hole is temporarily reduced by approximately 10 orders of magnitude out to a distance of approximately 0.1 pc . However, the gas quickly falls back to the centre of the potential well where again gas can be accreted at high rates driving another jet event.

4 SUMMARY & DISCUSSION

In this study we examine the impact of super-Eddington accretion and feedback on the growth rate of (supermassive) black hole seeds. In order to create SMSs, rapid accretion onto a proto-star is required, with accretion rates of close to $0.1 \text{ M}_{\odot}/\text{yr}$ thought to be necessary to inflate the envelope surrounding a proto-star and create a SMS. If such accretion rates can be maintained after the collapse of the SMS then super-Eddington accretion onto the seed black hole may be expected.

We here investigate exactly this scenario. We use the self-consistent SMS / massive PopIII simulations of R18 as a starting point for our simulations. The starting point is a massive PopIII star accreting at approximately $0.01 \text{ M}_{\odot}/\text{yr}$ with a final stellar mass of $15,904 \text{ M}_{\odot}$. To examine the subsequent accretion onto a seed black hole, we artificially collapse the massive PopIII star and create a direct collapse black hole seed. No supernova or other feedback from the massive PopIII star is modelled to precede the formation of a black hole. After black hole formation we model radiative feedback, below the ionisation threshold, and mechanical feedback in the form of bipolar jets for super-Eddington accretion events. We therefore focus almost entirely on the impact that jet feedback has on the growth of the black hole in this study. While radiative feedback could in principle regulate accretion to the Eddington rate we do not model this here. We instead choose to examine the impact of

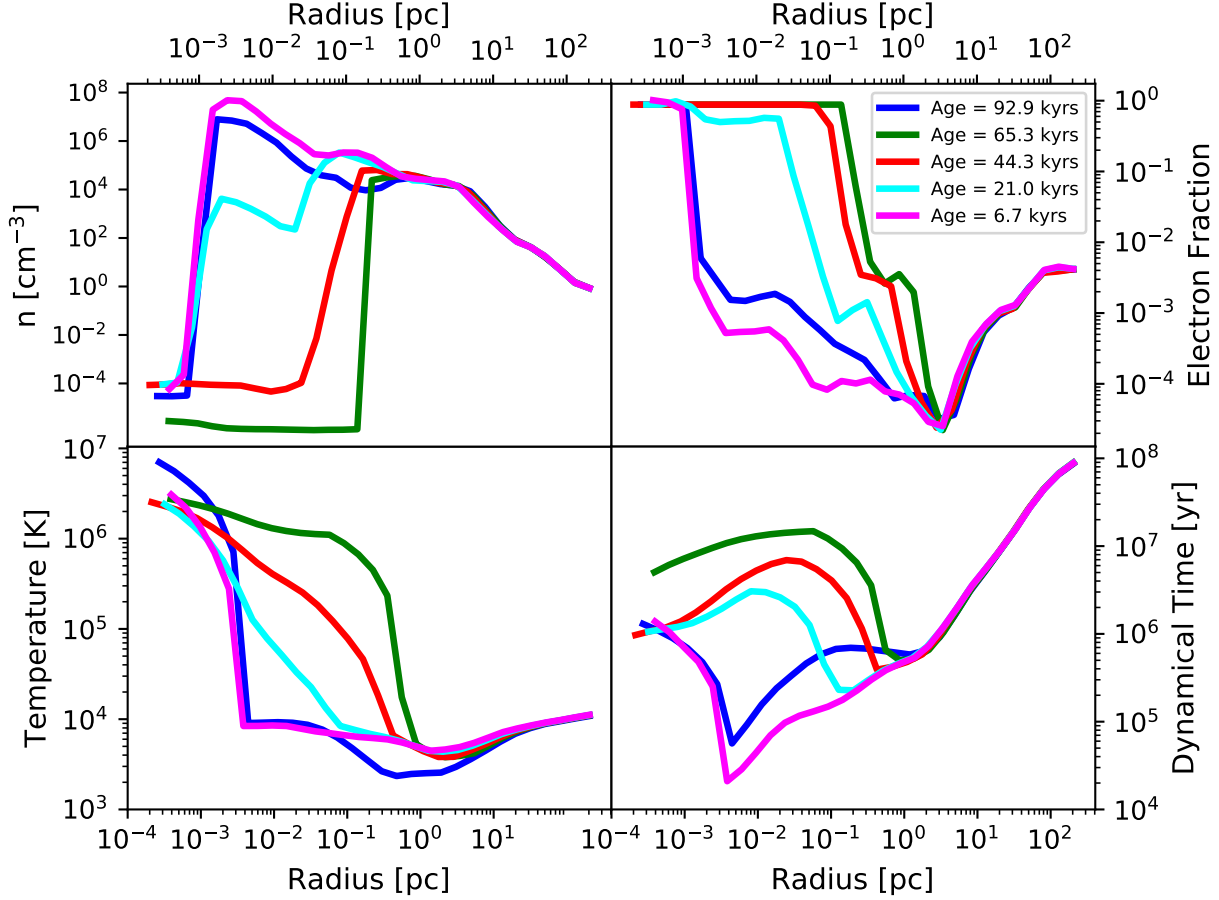


Figure 7. The same as Figures 5 and 6 for the $100,000 \text{ km s}^{-1}$ simulation. A similar pattern is observed. Jets are able to effectively drive gas away from the black hole severely suppressing growth. The gas recovery time can be as low as a few kiloyears for the highest densities.

super-Eddington accretion rates and the potential negative feedback associated with the jets driven by these extreme accretion rates. As discussed in §2.4.2 we launch bipolar jets at the maximum resolution our setup allows. The jets are launched by spreading the velocity of the jets equally over 27 cells just outside the accretion radius of our black hole. This corresponds to a physical resolution for the jet radius of approximately 300 au. This is still much coarser than the radius at which jets are launched by black holes of comparable sizes and hence our jets may still not be sufficiently collimated. This remains an inherent limitation of these simulations.

We modelled the bipolar jets using three different mass loading values. We modelled jets with velocities of $6,000 \text{ km s}^{-1}$ (0.018 c), $30,000 \text{ km s}^{-1}$ (0.1c) and $100,000 \text{ km s}^{-1}$ (0.33c). The results were qualitatively similar in each case. Periods of super-Eddington accretion generate violent bipolar jets which suppress accretion by many orders of magnitude. The gas surrounding the black hole is successfully evacuated and the gas must wait on the free-fall time before being available for accretion again. However, the jets are unable to break out of the very central region of the halo. The inflow is easily able to overwhelm the outflows. We see no impact from the jets at scales greater than approximately 1 pc and so the jets are found to be an inherently local phenomenon with no global impact for black holes of this mass ($\sim 19,000 M_{\odot}$). The local impact of the jets is significant and the jets successfully shut off the super-Eddington accretion that launched them initially, leading

to periods of low accretion immediately after jet launching, giving rise to episodic accretion as in the case of radiative feedback from light seeds (Milosavljević et al. 2009). These periods of inactivity lead to effective accretion a factor of a few below the Eddington rate.

The Eddington ratio, λ , can be used to describe accretion rates which are below Eddington. In Figure 8 we plot the growth rate of a black hole seed starting from the initial mass of the seed black hole studied here ($M_{\text{init}} = 15904 M_{\odot}$). The growth rate for a black hole seed is given by

$$M(t) = M(t_0) \exp(t/t_{\text{Edd}}) \quad (22)$$

where $M(t)$ is the mass after time t , $M(t_0)$ is the initial seed mass at $t_0 = 0$ and t_{Edd} is the Eddington (or Salpeter) time given by

$$t_{\text{Edd}} = \frac{\sigma_T \eta_{\text{disk}} c}{4\pi G m_p} \approx \eta_{\text{disk}} 5 \times 10^8 \text{ yr} \quad (23)$$

with η_{disk} the usual disk efficiency with canonical value 0.1. In this case the Eddington time for black hole is approximately 50 Myr. The growth of the black hole is then often counted in the number of e-folding times required to reach a predetermined mass. In Figure 8 we plot as dashed vertical lines the e-folding times for the seed black hole modelled here. The exponential nature of black hole growth means that initially growth is quite sedentary and only picks up as larger e-folding times are reached. The λ factor is used to describe growth rates which are below Eddington. In this study we found

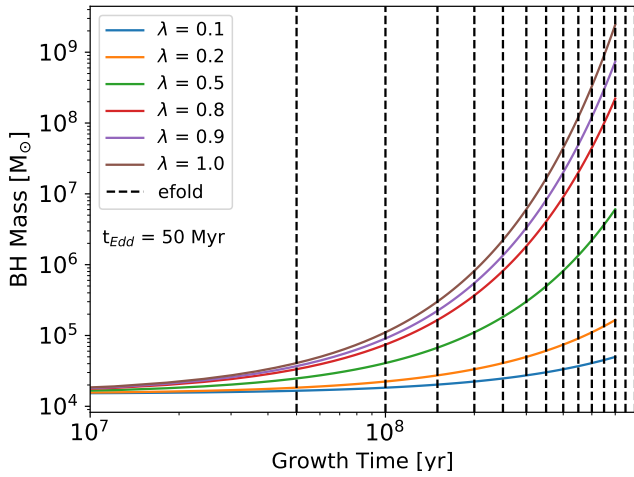


Figure 8. The Eddington limited growth rate of massive black holes for different values of the Eddington ratio, λ . The Eddington ratio is defined by $\lambda = \dot{M}_{BH} / \dot{M}_{Edd}$. Values of λ which deviate even moderately from 1.0 have significantly reduced growth. We find that mechanical feedback lead to an effective accretion rate approximately 0.25 times the canonical Eddington rate and hence an expected growth rate close to the orange line shown. The vertical dashed lines are the e-folding times determined from the Eddington time.

that the bipolar jets reduce growth to a factor of a few below the Eddington rate. We have also plotted these curves in our plot assuming that both η and λ are time independent. Growth rates which are a factor of two or more below Eddington have their mass, after 11 e-folding times, reduced by more than two orders of magnitude.

However, the black hole growth over longer times will likely be determined more by the dynamics of the host halo and its ability to merge with other haloes which may promote more efficient growth. If the black hole host halo is part of a number of major mergers this will undoubtedly promote more efficient accretion of material. Star formation in the surrounding gas will act to diminish growth by consuming available gas, although, we see no evidence of star formation in our simulations in the first 100,000 years after black hole formation.

If stars start to form and gas is enriched (internally or externally), the gas distribution will change. On the one hand, gas will be consumed in star formation. On the other hand, gas will cool more easily, fragment and generate regions of high and low density. If the cooling gas possesses angular momentum, it will settle in a disc from which the jet can more easily escape without damaging the surrounding if the jet propagates orthogonally to the disc (Cielo et al. 2018). If none of this happens and the halo grows by accreting metal-free intergalactic gas, perhaps the central density will be so high that the jet cannot do any damage even in its immediate surroundings and in this case super-Eddington accretion may well be possible for extended durations. Modelling the growth of seed black holes over several tens of megayears will require significantly more computational power and also the identification of realistic target haloes which form a seed in an environment which is favourable to rapid accretion at rates at or above the Eddington rate as the black hole grows. Such simulations are likely to be possible in the near future.

The idealised nature of our setup and the relatively short time for which we are able to evolve our simulations mean that we are

unable to provide more detailed information on the subsequent growth of the black hole. Nonetheless, accretion onto seed black holes formed from the direct collapse of a massive PopIII star is much more efficient than the accretion onto PopIII remnant black holes ($M_{init} \sim 100 M_{\odot}$) (e.g. Smith et al. 2018) which have initial accretion rates many orders of magnitude below the Eddington rate.

5 CONCLUSIONS

Mechanical feedback from bipolar jets is able to quickly evacuate high density gas from the accreting black hole once the accretion rate exceeds the canonical Eddington rate. However, the gas quickly recombines and falls back towards the centre of the potential on the freefall time of the system. The impact of the jet outflows is local to the immediate surroundings of the black hole. We find that the bipolar jets are unable to break out of the halo and indeed have no impact on scales greater than approximately 1 pc. Nonetheless, the jets have a significant impact on the black hole accretion rate. The effective accretion rate, taking into account periods of high accretion and intervening periods of quiescence, is reduced by a factor of a few below the Eddington accretion rate for at least the first 100,000 years after the formation of the black hole.

As an example, a reduction in the black hole accretion rate of a factor of 2 below the Eddington rate, if it were to remain at this level over the first 500 hundred million years of the black hole growth, would reduce the mass of the black hole by a factor of at least 20. The mass after 10 e-folding times would be between $10^5 M_{\odot}$ and $10^6 M_{\odot}$ assuming the black hole continues to accrete at half the Eddington rate. Therefore, direct collapse black holes born into atomic cooling haloes will require external influences (e.g. rapid major mergers with other haloes) to promote efficient accretion and reach SMBH masses within a few hundred million years. Further investigation of rapidly growing direct collapse host haloes will be required in the coming years to test the growth prospects of massive black hole seeds in realistic haloes.

ACKNOWLEDGEMENTS

J.A.R. acknowledges the support of the EU Commission through the Marie Skłodowska-Curie Grant - “SMARTSTARS” - grant number 699941. M.V. and A.L. acknowledge funding from the European Research Council under the European Community’s Seventh Framework Programme (FP7/2007-2013 Grant Agreement no. 614199, project “BLACK”). R.S.B acknowledges funding from the Centre National de la Recherche Scientifique (CNRS) on grant ANR-16-CE31-0011. Computations described in this work were performed using the publicly-available Enzo code (<http://enzo-project.org>), which is the product of a collaborative effort of many independent scientists from numerous institutions around the world. Their commitment to open science has helped make this work possible. The freely available astrophysical analysis code YT (Turk et al. 2011) was used to construct numerous plots within this paper. The authors would like to extend their gratitude to Matt Turk et al. for an excellent software package. J.A.R. would like to thank Lydia Heck and all of the support staff involved with Durham’s COSMA4 and DiRAC’s COSMA5 systems for their technical support. This work was supported by the Science and Technology Facilities Council (grant numbers ST/L00075X/1 and RF040365).

This work used the DiRAC Data Centric system at Durham University, operated by the Institute for Computational Cosmology on behalf of the STFC DiRAC HPC Facility (www.dirac.ac.uk). This equipment was funded by BIS National E-infrastructure capital grant ST/K00042X/1, STFC capital grant ST/H008519/1, and STFC DiRAC Operations grant ST/K003267/1 and Durham University. DiRAC is part of the National E-Infrastructure.

REFERENCES

- Abramowicz M. A., Fragile P. C., 2013, *Living Reviews in Relativity*, 16, 1
- Abramowicz M. A., Czerny B., Lasota J. P., Szuszkiewicz E., 1988, *ApJ*, 332, 646
- Alvarez M. A., Wise J. H., Abel T., 2009, *ApJ*, 701, L133
- Anninos W. Y., Norman M. J., 1994, *ApJ*, 429, 434
- Begelman M. C., Volonteri M., Rees M. J., 2006, *MNRAS*, 370, 289
- Begelman M. C., Rossi E. M., Armitage P. J., 2008, *MNRAS*, 387, 1649
- Bromm V., Loeb A., 2003, *ApJ*, 596, 34
- Bryan G. L., Norman M. L., O’Shea B. W., Abel T., Wise J. H., Turk M. J., The Enzo Collaboration, 2014, *ApJS*, 211, 19
- Chandrasekhar S., 1964, *ApJ*, 140, 417
- Chen P., Wise J. H., Norman M. L., Xu H., O’Shea B. W., 2014, *ApJ*, 795, 144
- Chon S., Hosokawa T., Yoshida N., 2017, *ArXiv e-prints*
- Cielo S., Bieri R., Volonteri M., Wagner A. Y., Dubois Y., 2018, *MNRAS*, 477, 1336
- Ciotti L., Ostriker J. P., 2001, *ApJ*, 551, 131
- Coppola C. M., Longo S., Capitelli M., Palla F., Galli D., 2011, *ApJS*, 193, 7
- Coppola C. M., D’Introno R., Galli D., Tennyson J., Longo S., 2012, *ApJS*, 199, 16
- Devecchi B., Volonteri M., 2009, *ApJ*, 694, 302
- Dijkstra M., Haiman Z., Mesinger A., Wyithe J. S. B., 2008, *MNRAS*, 391, 1961
- Dijkstra M., Ferrara A., Mesinger A., 2014, *MNRAS*, 442, 2036
- Doeleman S. S. et al., 2012, *Science*, 338, 355
- Done C., Davis S. W., Jin C., Blaes O., Ward M., 2012, *MNRAS*, 420, 1848
- Dubois Y., Pichon C., Haehnelt M., Kimm T., Slyz A., Devriendt J., Pogosyan D., 2012, *MNRAS*, 423, 3616
- Eisenstein D. J., Loeb A., 1995, *ApJ*, 443, 11
- Fan X. et al., 2006, *AJ*, 131, 1203
- Fernandez R., Bryan G. L., Haiman Z., Li M., 2014, *MNRAS*, 439, 3798
- Freitag M., Gürkan M. A., Rasio F. A., 2006, *MNRAS*, 368, 141
- Glover S. C. O., 2015a, *MNRAS*, 451, 2082
- Glover S. C. O., 2015b, *MNRAS*, 453, 2901
- Glover S. C. O., Abel T., 2008, *MNRAS*, 388, 1627
- Glover S. C. O., Jappsen A. K., 2007, *ApJ*, 666, 1
- Glover S. C. O., Savin D. W., 2009, *MNRAS*, 393, 911
- Gürkan M. A., Freitag M., Rasio F. A., 2004, *ApJ*, 604, 632
- Gürkan M. A., Fregeau J. M., Rasio F. A., 2006, *ApJ*, 640, L39
- Habouzit M., Volonteri M., Dubois Y., 2017, *MNRAS*, 468, 3935
- Haemmerlé L., Woods T. E., Klessen R. S., Heger A., Whalen D. J., 2017, *ArXiv e-prints*
- Haemmerlé L., Woods T. E., Klessen R. S., Heger A., Whalen D. J., 2018, *MNRAS*, 474, 2757
- Hahn O., Abel T., 2011, *MNRAS*, 415, 2101
- Heger A., Fryer C. L., Woosley S. E., Langer N., Hartmann D. H., 2003, *ApJ*, 591, 288
- Hirano S., Hosokawa T., Yoshida N., Kuiper R., 2017, *Science*, 357, 1375
- Hockney R. W., Eastwood J. W., 1988, *Computer simulation using particles*. Bristol: Hilger, 1988
- Hosokawa T., Omukai K., Yorke H. W., 2013a, *ApJ*, 778, 178
- Hosokawa T., Yorke H. W., Inayoshi K., Omukai K., Yoshida N., 2013b, *ApJ*, 778, 178
- Inayoshi K., Omukai K., 2012, *MNRAS*, 422, 2539
- Inayoshi K., Visbal E., Kashiyama K., 2015, *MNRAS*, 453, 1692
- Inayoshi K., Haiman Z., Ostriker J. P., 2016, *MNRAS*, 459, 3738
- Jiang Y. F., Stone J., Davis S. W., 2017, *ArXiv e-prints*
- Johnson J. L., Bromm V., 2007, *MNRAS*, 374, 1557
- Katz H., Sijacki D., Haehnelt M. G., 2015, *MNRAS*, 451, 2352
- Kim J. h., Wise J. H., Alvarez M. A., Abel T., 2011, *ApJ*, 738, 54
- Kitsionas S., Whitworth A. P., 2002, *MNRAS*, 330, 129
- Krumholz M. R., McKee C. F., Klein R. I., 2004, *ApJ*, 611, 399
- Latif M. A., Bovino S., Grassi T., Schleicher D. R. G., Spaans M., 2015, *MNRAS*, 446, 3163
- Lupi A., Haardt F., Dotti M., Fiacconi D., Mayer L., Madau P., 2016, *MNRAS*, 456, 2993
- Madau P., Haardt F., Dotti M., 2014, *ApJ*, 784, L38
- Mayer L., Kazantzidis S., Escala A., Callegari S., 2010, *Nature*, 466, 1082
- Mayer L., Fiacconi D., Bonoli S., Quinn T., Roškar R., Shen S., Wadsley J., 2015, *ApJ*, 810, 51
- Merloni A., Heinz S., 2008, *ArXiv e-prints*, 805
- Milosavljević M., Couch S. M., Bromm V., 2009, *ApJ*, 696, L146
- Miyoshi T., Kusano K., 2005, *Journal of Computational Physics*, 208, 315
- Mortlock D. J. et al., 2011, *Nature*, 474, 616
- O’Shea B. W., Abel T., Whalen D., Norman M. L., 2005, *ApJ*, 628, L5
- O’Shea B. W., Wise J. H., Xu H., Norman M. L., 2015, *ApJ*, 807, L12
- Pacucci F., Volonteri M., Ferrara A., 2015, *MNRAS*, 452, 1922
- Portegies Zwart S. F., Baumgardt H., Hut P., Makino J., McMillan S. L. W., 2004, *Nature*, 428, 724
- Regan J. A., Downes T. P., 2018a, *MNRAS*, 475, 4636
- Regan J. A., Downes T. P., 2018b, *MNRAS*, 478, 5037
- Regan J. A., Haehnelt M. G., 2009a, *MNRAS*, 396, 343
- Regan J. A., Haehnelt M. G., 2009b, *MNRAS*, 393, 858
- Regan J. A., Johansson P. H., Wise J. H., 2015, *MNRAS*, 449, 3766
- Regan J. A., Visbal E., Wise J. H., Haiman Z., Johansson P. H., Bryan G. L., 2017, *Nature Astronomy*, 1, 0075
- Sakurai Y., Inayoshi K., Haiman Z., 2016a, *MNRAS*, 461, 4496
- Sakurai Y., Vorobyov E. I., Hosokawa T., Yoshida N., Omukai K., Yorke H. W., 2016b, *MNRAS*, 459, 1137
- Sądowski A., 2009, *ApJS*, 183, 171
- Sądowski A., Narayan R., 2016, *MNRAS*, 456, 3929
- Sądowski A., Narayan R., McKinney J. C., Tchekhovskoy A., 2014, *MNRAS*, 439, 503
- Sądowski A., Lasota J. P., Abramowicz M. A., Narayan R., 2016, *MNRAS*, 456, 3915
- Schauer A. T. P., Regan J., Glover S. C. O., Klessen R. S., 2017, *MNRAS*, 471, 4878
- Schleicher D. R. G., Palla F., Ferrara A., Galli D., Latif M., 2013, *A&A*, 558, A59
- Smith B. D., Regan J. A., Downes T. P., Norman M. L., O’Shea B. W., Wise J. H., 2018, *MNRAS*, 480, 3762

- Smith B. D. et al., 2017, MNRAS, 466, 2217
- Stone J. M., Norman M. L., 1992a, ApJS, 80, 753
- Stone J. M., Norman M. L., 1992b, ApJS, 80, 791
- Sugimura K., Omukai K., Inoue A. K., 2014, MNRAS, 445, 544
- Tanaka T. L., Li M., 2014, MNRAS, 439, 1092
- Toyouchi D., Hosokawa T., Sugimura K., Nakatani R., Kuiper R., 2018, ArXiv e-prints, [arXiv:1811.01368](https://arxiv.org/abs/1811.01368)
- Tselikhovich D., Hirata C., 2010, Phys. Rev. D, 82, 083520
- Turk M. J., Smith B. D., Oishi J. S., Skory S., Skillman S. W., Abel T., Norman M. L., 2011, ApJS, 192, 9
- Visbal E., Haiman Z., Bryan G. L., 2014, MNRAS, 445, 1056
- Whalen D., Abel T., Norman M. L., 2004, ApJ, 610, 14
- Wise J. H., Abel T., 2011, MNRAS, 414, 3458
- Wolcott-Green J., Haiman Z., 2012, MNRAS, 425, L51
- Woods T. E., Heger A., Whalen D. J., Haemmerlé L., Klessen R. S., 2017, ApJ, 842, L6
- Woosley S. E., Heger A., Weaver T. A., 2002, Reviews of Modern Physics, 74, 1015
- Xu H., Wise J. H., Norman M. L., 2013, ApJ, 773, 83

This paper has been typeset from a \TeX / \LaTeX file prepared by the author.